Electronic Supplementary Information to: Modeling the impedance response and steady state behaviour of porous CGO-based MIEC anodes

Philip Marmet,*[a] Lorenz Holzer,[a] Jan G. Grolig,[b] Holger Bausinger,[b] Andreas Mai,[b] Joseph M. Brader,[c] and Thomas Hocker[a]

[a] *Zurich University of Applied Sciences, Institute of Computational Physics, Winterthur, Switzerland.*
Tel: +41 (0)58 934 70 80; E-mail: mame@zhaw.ch
[b] *Hexis AG, Winterthur, Switzerland.*
[c] *Department of Physics, University of Fribourg, Fribourg, Switzerland.*

Contents

*

A Calculation of the oxygen partial pressure from gas-phase equilibrium

In order to use these p_{O_2} dependent material laws, the local p_{O_2} is estimated from the gas-phase equilibrium of the local atmospheric conditions. The p_{O_2} depends on the H_2 and H_2O concentrations according to the dissociation of water:

$$2H_2O \Leftrightarrow 2H_2 + O_2 \tag{1}$$

The equilibrium constant of this reaction is given by[1]:

$$K_p(T) = \exp\left(\frac{G^0}{RT}\right) = \frac{(p_{H_2O})^2}{(p_{H_2})^2 p_{O_2}} \tag{2}$$

The temperature dependent Gibbs free energy G^0 of the reaction can be derived from Shomate parameters as described by Linder et al.[2] on a kJ/mol basis for $T \geq 373.15\,\mathrm{K}$:

$$G^0 = -241.2 + 38.24 \cdot 10^{-3} T + 14.15 \cdot 10^{-6} T^2 - 3.722 \cdot 10^{-9} T^3 \tag{3}$$

Therewith, the oxygen partial pressure p_{O_2} at a given temperature can be calculated from the partial pressures of hydrogen and water:

$$p_{O_2} = \left(\frac{p_{H_2O}}{p_{H_2}}\right)^2 \frac{1}{K_p(T)} \tag{4}$$

B Dusty-gas model (DGM) for the gas transport in the MIEC-pores

Within the porous MIEC anode, the transport and the reaction of the gas species needs to be described. The continuity equations for the gas species reads:

$$\varepsilon_{\mathrm{pore}} \frac{\partial c_1}{\partial t} + \nabla \cdot N_1 = R_1 \tag{5}$$

$$\varepsilon_{\mathrm{pore}} \frac{\partial c_2}{\partial t} + \nabla \cdot N_2 = R_2 \tag{6}$$

where c_1, c_2 are the molar concentrations, N_1, N_2 are the molar flux densities and R_1, R_2 are the reaction rates for hydrogen (species 1) and water vapour (species 2) , respectively. Thereby, the consumption rate of hydrogen is equal to the production rate of water vapour, which is equal to the production rate of oxygen ion vacancies:

$$R_2 = -R_1 = R_{\mathrm{vac}}, \tag{7}$$

where R_{vac} is defined in Eq. 11 of the research article. The corresponding boundary conditions for the continuity equations 5 and 6 are documented in section 2.3.10 of the research article.

For the molar flux densities N_1 and N_2, the effect of the porous microstructure needs to be considered. In nanoporous materials, gas diffusion is controlled by collision of gas molecules with the pore walls. In this case the mean free path of the gas molecules is longer than the characteristic length of the pores so that we enter the Knudsen diffusion regime. Modern high performance MIEC electrodes are usually very fine-grained in order to increase the specific surface area and associated reactivity. In most cases, the pore size in modern MIEC electrodes is in the μm to sub-μm scale, where both Knudsen and bulk diffusion become relevant. It is generally agreed[3–5] that the dusty-gas model (DGM) is the most convenient approach for modelling combined bulk and Knudsen diffusion. Therefore, in our approach, the diffusion in the porous CGO-layer is modelled with the dusty-gas model.

The DGM is an extension of the Stefan Maxwell model, where the pore phase (="dust") is treated as an additional, stationary species. Helpful explanations and different versions of the DGM can be found in these references[3,6–8] for the interested reader. The original DGM for a binary gas mixture can be expressed as follows[6]:

$$\begin{aligned} &\frac{N_1}{D_{1\mathrm{Kn,eff}}} + \frac{x_2 N_1 - x_1 N_2}{D_{12,\mathrm{eff}}} \\ &= -\frac{1}{R_{\mathrm{gas}} T}\left(p \nabla x_1 + x_1 \nabla p + x_1 \nabla p \frac{k_{\mathrm{flow}}\, p}{D_{1\mathrm{Kn,eff}}\, \mu_{\mathrm{visc}}}\right) \end{aligned} \tag{8}$$

$$\frac{N_2}{D_{2\mathrm{Kn,eff}}} + \frac{x_1 N_2 - x_2 N_1}{D_{12,\mathrm{eff}}} = -\frac{1}{R_{\mathrm{gas}} T}\left(p\nabla x_2 + x_2 \nabla p + x_2 \nabla p \frac{k_{\mathrm{flow}}\, p}{D_{2\mathrm{Kn,eff}}\, \mu_{\mathrm{visc}}}\right) \tag{9}$$

where x_1, x_2 are the molar fractions for hydrogen and water, respectively. Furthermore, p is the pressure, k_{flow} the gas-flow permeability and μ_{visc} the dynamic viscosity of the gas mixture. Note that the dynamic viscosity of hydrogen is used as an approximation for the viscosity of the gas mixture, valid for low water fractions. $D_{1\mathrm{Kn,eff}}$ and $D_{2\mathrm{Kn,eff}}$ are the effective Knudsen diffusion coefficients for the hydrogen and water and $D_{12,\mathrm{eff}}$ is the binary diffusion coefficient between hydrogen and water. The diffusion coefficients are determined in section C.

An explicit version of the DGM for a binary system was derived by Liu et al.[6] and reads:

$$N_1 = -\frac{D_{12,\mathrm{eff}} D_{1\mathrm{Kn,eff}}}{D_{12,\mathrm{eff}} + x_1 D_{2\mathrm{Kn,eff}} + x_2 D_{1\mathrm{Kn,eff}}} \nabla c_1 - \frac{D_{1\mathrm{Kn,eff}} D_{2\mathrm{Kn,eff}}}{D_{12,\mathrm{eff}} + x_2 D_{1\mathrm{Kn,eff}} + x_1 D_{2\mathrm{Kn,eff}}} \frac{x_1 \nabla p}{R_{\mathrm{gas}} T} - c_1 \frac{k_{\mathrm{flow}}}{\mu_{\mathrm{visc}}} \nabla p \tag{10}$$

$$N_2 = -\frac{D_{12,\mathrm{eff}} D_{2\mathrm{Kn,eff}}}{D_{12,\mathrm{eff}} + x_1 D_{2\mathrm{Kn,eff}} + x_2 D_{1\mathrm{Kn,eff}}} \nabla c_2 - \frac{D_{2\mathrm{Kn,eff}} D_{1\mathrm{Kn,eff}}}{D_{12,\mathrm{eff}} + x_1 D_{2\mathrm{Kn,eff}} + x_2 D_{1\mathrm{Kn,eff}}} \frac{x_2 \nabla p}{R_{\mathrm{gas}} T} - c_2 \frac{k_{\mathrm{flow}}}{\mu_{\mathrm{visc}}} \nabla p \tag{11}$$

where c_1 and c_2 are the molar concentrations of hydrogen and water vapour, respectively. To achieve a better overview, the terms in Eqs. 10 and 11 can be separated into diffusive and convective parts. Starting from Eq. 10 and Eq. 11, the terms of the binary DGM model can be summarized in diffusive and convective parts with summarized diffusion coefficients as derived by Liu et al.[6]:

$$N_1 = N_{1,\mathrm{diff}} + N_{1,\mathrm{conv}} \tag{12}$$

$$= -D_{\mathrm{DG1}} \nabla c_1 + c_1 u \tag{13}$$

$$N_2 = N_{2,\mathrm{diff}} + N_{2,\mathrm{conv}} \tag{14}$$

$$= -D_{\mathrm{DG2}} \nabla c_2 + c_2 u \tag{15}$$

Thereby, the convective gas velocity can be formulated as:

$$u = \left(\frac{1}{R_{\mathrm{gas}} T c_{\mathrm{tot}}} D_{\mathrm{DG3}} + \frac{k_{\mathrm{flow}}}{\mu_{\mathrm{visc}}}\right) \nabla p \tag{16}$$

The summarized diffusion coefficients read:

$$D_{\mathrm{DG1}} = \frac{D_{12,\mathrm{eff}} D_{1\mathrm{Kn,eff}}}{D_{12,\mathrm{eff}} + x_1 D_{2\mathrm{Kn,eff}} + x_2 D_{1\mathrm{Kn,eff}}} \tag{17}$$

$$D_{\mathrm{DG2}} = \frac{D_{12,\mathrm{eff}} D_{2\mathrm{Kn,eff}}}{D_{12,\mathrm{eff}} + x_1 D_{2\mathrm{Kn,eff}} + x_2 D_{1\mathrm{Kn,eff}}} \tag{18}$$

$$D_{\mathrm{DG3}} = \frac{D_{1\mathrm{Kn,eff}} D_{2\mathrm{Kn,eff}}}{D_{12,\mathrm{eff}} + x_1 D_{2\mathrm{Kn,eff}} + x_2 D_{1\mathrm{Kn,eff}}} \tag{19}$$

The pressure and thus the pressure gradient is linked to the total molar gas concentration c_{tot} through the ideal gas

law:

$$p = c_{\text{tot}} R_{\text{gas}} T \tag{20}$$

$$\nabla p = R_{\text{gas}} T \nabla c_{\text{tot}} \tag{21}$$

$$\text{where} \quad c_{\text{tot}} = c_1 + c_2 \tag{22}$$

C Determination of the diffusion coefficients

For the DGM and for the Stefan-Maxwell model, the binary diffusion coefficients need to be determined. Todd and Young[9] studied different approaches for the determination of binary diffusion coefficients and concluded that the approach according to Fuller et al.[10] provides the most accurate results for the temperature range relevant for SOFC's with an estimated mean error of 5% and a maximum error of about 20%. The diffusion coefficients according to Fuller et al.[10] read:

$$D_{12,0} = \frac{0.00143\, T^{1.75}}{p M_{12}^{1/2} \left(V_1^{1/3} + V_2^{1/3} \right)^2} \tag{23}$$

with

$$M_{12} = (1/M_1 + 1/M_2)^{-1} \tag{24}$$

where M_i is the molecular mass and V_i the diffusion volume. These parameters are summarized in table 1 for hydrogen and water vapour.

Table 1 Parameters for the calculation of the binary diffusion coefficients[9]

Gas species	Molar mass M_i	diffusion volume V_i	Molecular diameter d_{Molec}
H_2	2.016 kg/kmol	6.12	2.40 Å
H_2O	18.015 kg/kmol	13.10	2.75 Å

To account for the effect of the microstructure, the binary diffusion coefficient needs to be corrected to get the effective transport property:

$$D_{12,\text{eff}} = M_{\text{pore}} D_{12,0} \tag{25}$$

where the microstructure factor M_{pore} for the pore phase is defined in Eq. 4 of the research article.

The intrinsic Knudsen diffusion coefficient using the kinetic theory of gases is given by[11]:

$$D_{i,\text{Kn},0} = \frac{1}{3} d_{\text{pore}} \bar{v} \tag{26}$$

$$\bar{v} = \sqrt{\frac{8 k_B T}{M_i \pi}} \tag{27}$$

where $\bar{v}$ is the mean thermal velocity and d_{pore} is a characteristic pore diameter of the porous structure.

To account for the effect of the microstructure, the intrinsic Knudsen diffusion coefficients need to be corrected to get the effective Knudsen diffusion coefficients:

$$D_{i\text{Kn,eff}} = M_{\text{pore,Kn}} D_{i\text{Kn},0}. \tag{28}$$

Thereby, i denotes species 1 (hydrogen) or 2 (water vapour) and $M_{\text{pore,Kn}}$ is the microstructure factor for the Knudsen diffusion mechanism. Note that the intrinsic Knudsen diffusion coefficient $D_{i,\text{Kn},0}$ in Eq. 26 accounts for the effect of the scattering with the walls of the small pores, but not for the microstructure characteristic itself. An appropriate picture for the intrinsic Knudsen diffusion illustrated in Fig. 1 a) is a small pipe with diameter d_{pore}, porosity $\varepsilon_{\text{pore}} = 1$, tortuosity $\tau_{\text{pore}} = 1$ and without bottlenecks i.e. $\beta_{\text{pore}} = 1$, resulting in an M-factor $M_{\text{pore,Kn}} = 1$. In the presence of a porous microstructure as illustrated in Fig. 1 b), the Knudsen diffusion will be additionally hindered due to porosity $\varepsilon_{\text{pore}} < 1$, tortuous pathways and bottlenecks, resulting in an M-factor $M_{\text{pore,Kn}} < 1$. However, a quantitative relationship between the microstructure

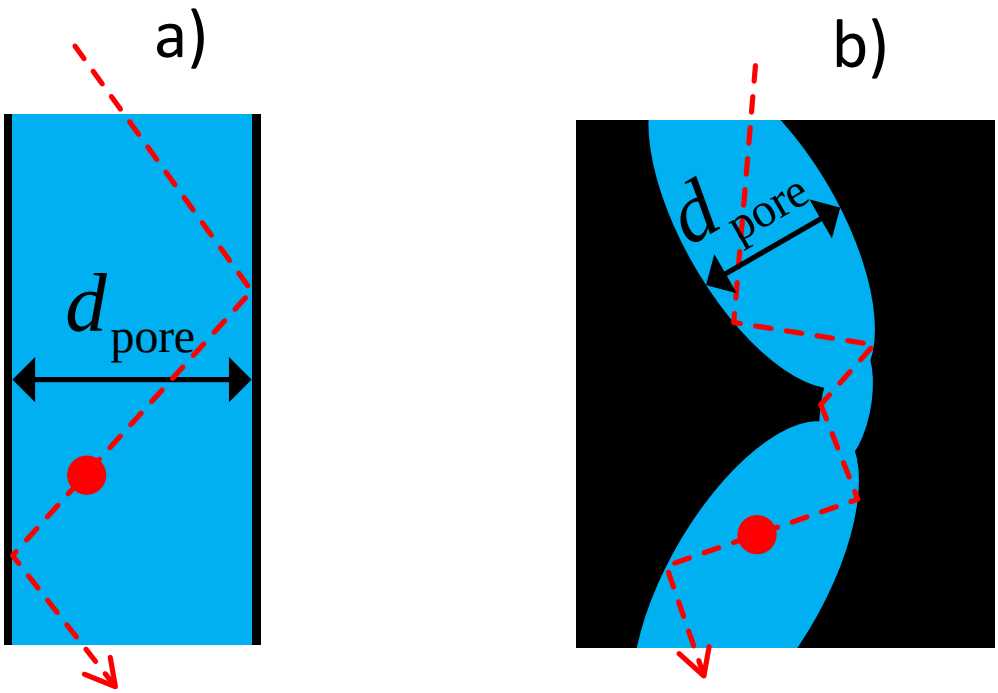

Fig. 1 Illustration of the microstructure effects on the Knudsen diffusion: a) intrinsic Knudsen diffusion with $M_{\mathrm{pore,Kn}} = 1$, b) effective Knudsen diffusion with $M_{\mathrm{pore,Kn}} < 1$ due to porosity $\varepsilon_{\mathrm{pore}} < 1$, tortuous pathways and bottlenecks.

parameters $\varepsilon_{\mathrm{pore}}$, τ_{pore} and β_{pore} like for the bulk diffusion in equation 4 of the research article is not available for the Knudsen diffusion yet. The "bulk" microstructure factor M_{pore} and the Knudsen structure factor $M_{\mathrm{pore,Kn}}$ might be similar, but not necessarily equal, as different processes are hindering the transport for the two transport mechanisms. Therefore, the microstructure factor $M_{\mathrm{pore,Kn}}$ for Knudsen diffusion needs to be determined indirectly, for example, by running a suitable transport simulation, for which we use the GeoDict[12] software. In GeoDict, $M_{\mathrm{pore,Kn}}$ is determined using a random walk method. Moreover, the characteristic pore diameter d_{pore} of the porous structure in Eq. 26 is not a well defined quantity and is therefore determined from the random walk simulation as the mean path length between two consecutive hits of molecule and wall.

D Knudsen number

Even if the binary diffusion coefficients are needed for the model, the unitary diffusion coefficients are helpful as a reference and enable the calculation of the Knudsen number. The unitary diffusion coefficient according to the kinetic theory of gases reads[13]:

$$D_{\mathrm{bulk},0} = \frac{1}{3}\lambda\bar{v} \tag{29}$$

$$\lambda = \frac{k_B T}{\sqrt{2}\pi d_{\mathrm{Molec}}^2 p} \tag{30}$$

where λ is the mean free path between collisions of gas molecules, $\bar{v}$ the mean thermal velocity and d_{Molec} is the diameter of the molecule. The Knudsen number is the ratio of the transport by bulk diffusion to the Knudsen diffusion and therewith the ratio of the mean free path and the pore diameter:

$$Kn_{i,0} = \frac{D_{i,0}}{D_{i\mathrm{Kn},0}} = \frac{\lambda}{d_{\mathrm{pore}}} \tag{31}$$

Depending on the Knudsen number we end up with three different transport regimes:

- $Kn << 1$: dominated by bulk diffusion
- $Kn \approx 1$: by bulk and by Knudsen diffusion
- $Kn >> 1$: dominated by Knudsen diffusion

As mentioned, the M-factor for the Knudsen diffusion can differ from the M-factor for the bulk-diffusion. We can thus formulate an effective Knudsen number Kn_{eff} relating the effective bulk and Knudsen diffusivity in the same manner as in equation 31:

$$Kn_{i,\text{eff}} = \frac{D_{\text{i,eff}}}{D_{i\text{Kn,eff}}} = Kn_{i,0} \cdot \frac{M_{\text{pore}}}{M_{\text{pore,Kn}}} \tag{32}$$

The effective Knudsen number Kn_{eff} also accounts for the different influences of the microstructures on the bulk and Knudsen diffusion.

E Stefan-Maxwell formulation for the gas transport in the stagnant gas layer

There is a stagnant gas layer above the electrode, where the gas transport is governed by diffusion and not by convection of the excess fuel supply. The thickness of this stagnant gas layer strongly depends on the flowrate and on the experimental setup of the button cell. For our standard simulations, a quite small stagnant gas layer thickness of $L_{\text{Stag}} = 0.2\text{mm}$ is used. This value was estimated from a flow simulation of a particular stagnation point-flow like setup (see SM section C).

The continuity equation for the stagnant gas layer reads:

$$\frac{\partial c_1}{\partial t} + \nabla \cdot N_1 = 0 \tag{33}$$

$$\frac{\partial c_2}{\partial t} + \nabla \cdot N_2 = 0 \tag{34}$$

where N_1, N_2 are the molar flux densities for hydrogen and water vapour, respectively. Boundary conditions are documented in section 2.3.10 of the research article.

The diffusion in the stagnant gas layer is modelled with the Stefan-Maxwell[3,7] equations with the following assumptions:

- The relation $N_2 = -N_1$ for the water vapour and hydrogen fluxes respectively is used, in conjunction with the relation $x_2 = 1 - x_1$. Both relations are valid in the absence of any chemical reactions.
- The influence of the pressure gradient for the diffusive flux is neglected.

With these assumptions, the original Stefan-Maxwell equations can be simplified to the following explicit expressions for the hydrogen and water vapour fluxes, respectively:

$$N_1 = -\frac{D_{12,\text{eff}}}{R_{\text{gas}} T} p \nabla x_1 = -D_{12,\text{eff}} \nabla c_1 \tag{35}$$

$$N_2 = -\frac{D_{12,\text{eff}}}{R_{\text{gas}} T} p \nabla x_2 = -D_{12,\text{eff}} \nabla c_2. \tag{36}$$

In the following, the derivation of this simplified version of the Stefan-Maxwell is presented. The original Stefan-Maxwell[3,7] equations for a binary mixture reads:

$$\frac{x_2 N_1 - x_1 N_2}{D_{12,\text{eff}}} = -\frac{1}{R_{\text{gas}} T} \left(p \nabla x_1 + x_1 \nabla p \right) \tag{37}$$

$$\frac{x_1 N_2 - x_2 N_1}{D_{12,\text{eff}}} = -\frac{1}{R_{\text{gas}} T} \left(p \nabla x_2 + x_2 \nabla p \right) \tag{38}$$

Using $N_2 = -N_1$ and $x_2 = 1 - x_1$ we get:

$$\frac{(1-x_1)N_1 + x_1 N_1}{D_{12,\text{eff}}} = -\frac{1}{R_{\text{gas}}T}\left(p\nabla x_1 + x_1 \nabla p\right) \tag{39}$$

We can solve for N_1:

$$N_1 = -\frac{D_{12,\text{eff}}}{RT}\left(p\nabla x_1 + x_1 \nabla p\right) \tag{40}$$

We neglect the influence of the pressure gradient for the diffusive flux and therewith we get relations for N_1 and N_2 respectively, used in section E , which are repeated here for completeness:

$$N_1 = -\frac{D_{12,\text{eff}}}{R_{\text{gas}}T} p \nabla x_1 = -D_{12,\text{eff}} \nabla c_1 \tag{41}$$

$$N_2 = -\frac{D_{12,\text{eff}}}{R_{\text{gas}}T} p \nabla x_2 = -D_{12,\text{eff}} \nabla c_2 \tag{42}$$

Because of the different molar masses of hydrogen and water, an equal molar flux leads to a higher water mass flux than hydrogen mass flux. Therewith, a convective part for transport is needed. The associated gas-flow velocity in the stagnant gas layer is the so-called Stefan-velocity u and obeys the continuity equation:

$$\nabla \cdot (\rho u) = R_1 + R_2 \tag{43}$$

As the reaction terms are zero in the stagnant gas layer, the velocity u is constant and can be expressed as:

$$u = \frac{N_1 M_1 + N_2 M_2}{\rho} \tag{44}$$

The presence of a convective velocity gives rise to a pressure gradient according to darcy's law. However, as we neglect the influence of this pressure gradient on the diffusive transport, the convective and the diffusive fluxes are decoupled. Therewith, the velocity in the stagnant gas layer can be determined as a post-processing property. This is in contrast to the gas-flow velocity in the porous MIEC-layer, where the full coupling is accounted for based on the DGM.

F Estimation of the stagnant gas layer thickness

To estimate the stagnant gas layer thickness, a CFD flow simulation is performed for the specific axial-symmetric setup shown in Fig. 2 a). The inflow velocity is prescribed as $v_{\text{in}} = 0.023\,\text{m/s}$, which corresponds to a flowrate of $200\,\text{ml/min}$. The resulting flowfield and streamlines are shown in Fig. 2 b).

As an estimation of the thickness of the stagnant gas layer, the zone above the electrode where the viscous forces F_{visc} exceed the inertia forces F_{inertia} is used. In this zone, the gas transport will be dominated by diffusion and not by convection. The viscous and the inertia forces are given by:

$$F_{\text{visc}} = \mu_{\text{visc}} \dot{\gamma} \tag{45}$$

$$F_{\text{inertia}} = \left|\rho\left(\vec{v}\cdot\nabla\right)\vec{v}\right| \tag{46}$$

where μ_{visc} is the dynamic viscosity, $\dot{\gamma}$ the shear rate, ρ the density of hydrogen and $\vec{v}$ the gas velocity.

In Fig. 2 c), the region where the diffusion dominates over the convective transport (i.e. $F_{\text{visc}} > F_{\text{inertia}}$) is colored in red. From this plot, a stagnant gas layer thickness of about 0.2 mm can be estimated. Note that the stagnant gas layer thickness strongly depends on the flowrate and the experimental setup!

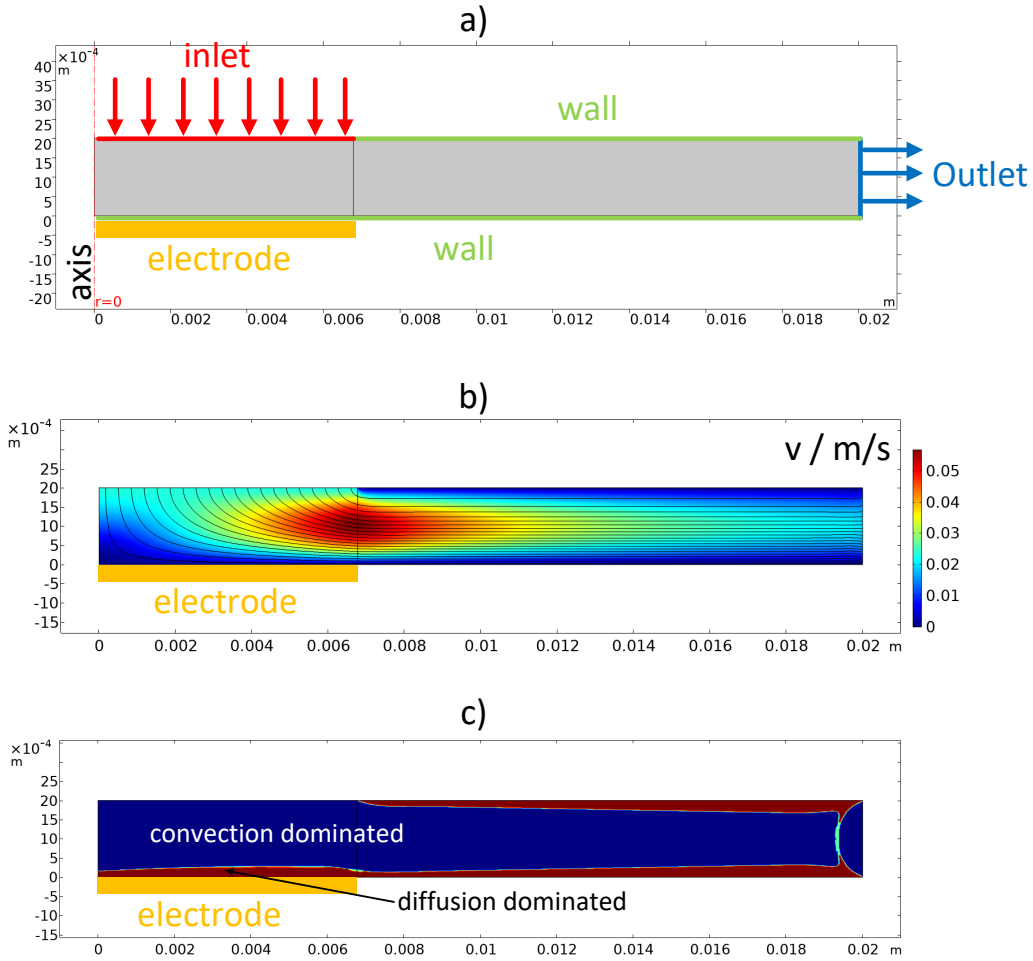

Fig. 2 Axialsymmetric CFD flow simulation using Comsol Multiphysics to estimate the stagnant gas layer thickness: a) dimension and boundary conditions of the setup, b) flowfield and streamlines c) Indication of convection dominated (blue) and diffusion dominated (red) gas transport regimes.

G Derivation of the averaging of the surface reaction overpotential

Note that the surface reaction overpotential η_{SR} is a distributed quantity which varies along the CGO-layer thickness. To yield an effective overpotential $\eta_{\mathrm{SR,eff}}$ due to the total surface reaction process, we first formulate the power loss $P_{\mathrm{tot}} = UI$ associated with the surface reaction process:

$$P_{\mathrm{tot}} = \int_0^L \eta_{\mathrm{SR}} i_{\mathrm{SR}} A_{\mathrm{1D}} dx \tag{47}$$

where A_{1D} is the cross section of the 1D simulation in the y-z-plane. For convenience, we reformulate to a power density:

$$p_{\mathrm{tot}} = \frac{P_{\mathrm{tot}}}{A_{\mathrm{1D}}} = \int_0^L \eta_{\mathrm{SR}} i_{\mathrm{SR}} dx \tag{48}$$

To get the averaged surface reaction overpotential $\eta_{\mathrm{SR,avg}}$, we can simply divide the power density by the average current density J_{charge} to get the final expression Eq. 37 of the research article, which is repeated here for convenience:

$$\eta_{\mathrm{SR,avg}} = \frac{p_{\mathrm{tot}}}{J_{\mathrm{charge}}} = \frac{1}{J_{charge}} \int_0^L \eta_{\mathrm{SR}} i_{\mathrm{SR}} dx \tag{49}$$

H Fit function for the oxygen-nonstoichiometry δ

The fit function used to describe the oxygen-nonstoichiometry δ as a function of the temperature T and the oxygen partial pressure p_{O_2} for the experimental date discussed in section 2.4.2 of the research article is expressed as:

$$\begin{aligned} \log(\delta) = &-\frac{1}{4}(\log_{10}(p_{O_2}) + b_T) \\ &+min\left(b_1\left(\log_{10}(p_{O_2}) - b_{T0} + b_T + \frac{b_2}{b_1}\right), 0\right) \end{aligned} \tag{50}$$

With the parameters:

$$b_T = a_{T1}T^2 + a_{T2}T + a_{T3} \tag{51}$$

$$b_{T0} = a_{T1}T_0^2 + a_{T2}T_0 + a_{T3} \tag{52}$$

$$T_0 = 1273.15\,\mathrm{K}$$

$$a_{T1} = 3.754717722603253e-05 \tag{53}$$

$$a_{T2} = -0.120640040021060 \tag{54}$$

$$a_{T3} = 1.116305561104715e+02 \tag{55}$$

$$b_1 = 0.159431946658546 \tag{56}$$

$$b_2 = 2.357177536920600 \tag{57}$$

A reasonable agreement of the fit function to the experimental data is achieved as shown in Fig. 5 in section 2.4.2 of the research article , which is sufficient for the purpose of the current study.

I Calculation of the mobility and diffusivity of the charge carriers

The conductivity of the charge carriers is related to the mobility μ according to Eq. 53 of the research article. As the charge carriers are assumed to be transported by drift and diffusion according to Eqs. 5 and 6 of the research article, the mobility and diffusivity of the charge carriers is required. Therefore, the mobility of vacancies and electrons is determined using Eq. 53, Eq. 51 and Eq. 52 of the research article with a reference oxygen partial pressure of $p_{O_2,\mathrm{ref}} = 10^{-19}\,\mathrm{bar}$ and a reference temperature of $T_{\mathrm{ref}} = 850\,^{\circ}\mathrm{C}$.

$$\mu_{\mathrm{eon}} = \frac{\sigma_{\mathrm{eon}}(T_{\mathrm{ref}}, p_{O_2,\mathrm{ref}})}{F^2\, c_{\mathrm{eon,eq}}(p_{O_2,\mathrm{ref}})} \tag{58}$$

$$\mu_{\mathrm{vac}} = \frac{\sigma_{\mathrm{eon}}(T_{\mathrm{ref}}, p_{O_2,\mathrm{ref}})}{F^2\, c_{\mathrm{vac,eq}}(p_{O_2,\mathrm{ref}})} \tag{59}$$

where $c_{\mathrm{eon,eq}}$ and $c_{\mathrm{vac,eq}}$ are defined in Eqs. 48 and 49 of the research article. The corresponding diffusivities of the charge cariers in CGO10 are then calculated with the Nernst-Einstein relation Eq. 7 and are reported in table 1 of the research article. Note that the ${p_{O_2}}^{-1/4}$-dependency is included in the drift-diffusion Eqs. 5 and 6 of the research article due to the multiplication of the mobility with the charge carrier concentrations, which depends on the oxygen-nonstoichiometry. However, the oxygen-nonstoichiometry δ does not simply show a ${p_{O_2}}^{-1/4}$-dependency over the whole range, i.e. for oxygen-nonstochiometries of $\log(\delta) > -1$, the linear dependency deviates from ${p_{O_2}}^{-1/4}$ (see Fig. 5 of the research article). However, in the current study, the fuel composition is not varied and the operating point is in a range where the ${p_{O_2}}^{-1/4}$-relation holds.

According to the drift-diffusion Eq. 5 of the research article, a dependency of the ionic conductivity on the p_{O_2} is

assumed via the multiplication of the vacancy concentration with their mobility. However, no such dependency is reported for the ionic conductivity by Steele[14] as expressed in Eq. 51 of the research article. From Yasuda et al.[15] a similar relation for the ionic conductivity without dependency on the oxygen partial pressure is suggested. In contrast, Wang et al.[16] suggested that the ionic conductivity might show a ${p_{O_2}}^{-1/4}$-dependency according to the additional vacancies introduced for low oxygen partial pressures. For simplicity, we follow the assumptions of Wang et al.[16], which are consistent with our model assumptions according to Eqs. 5 and 6 of the research article, assuming the vacancy transport by drift to be proportional to the vacancy concentration c_{vac}.

J Estimation of the exchange reaction rate k_0

The exchange reaction rate k_0 is hard do be estimated from EIS measurements in a reliable way, because of the influence of the microstructure and because of the overlapping processes of e.g. gas concentration impedance. Gerstl et al.[17] conducted thin-film model electrode experiments with CGO20, reporting an initial surface reaction resistance of $ASR_{\mathrm{SR,TF}} = 10\,\Omega\mathrm{cm}^2$ operated in an atmosphere $x_1 = 2.5\%$ and $x_2 = 2.5\%$ in Ar.

For our estimation we now assume that the surface reaction resistance per surface area for CGO20 thin-film electrodes is in the same range as for porous CGO10 electrodes. With this approach, we can simply scale the resistance to the much higher porous surface of the porous CGO electrode. According to the microstructure analysis, the pore surface area per porous layer is $S = 2.68\,\mu^2\mathrm{m}/\mu^3\mathrm{m}$. Multiplying by the CGO-layer thickness, we get the pore surface area per cell-surface area:

$$S_{\mathrm{tot}} = SL \tag{60}$$

Assuming a uniform distribution of the reaction, we can now estimate the surface reaction resistance of the porous electrode for a electrode CGO-layer thickness of $L = 100\mu\mathrm{m}$:

$$ASR_{\mathrm{SR,porous}} = \frac{R_{\mathrm{SR,TF}}}{S_{\mathrm{tot}}} = \frac{R_{\mathrm{SR,TF}}}{S_{\mathrm{3D}}L} = 0.037\Omega cm^2 \tag{61}$$

The exchange reaction rate is now tuned to result in approximately this value for the surface reaction resistance ASR_{SR} as shown in Fig. 10 of the research article.

Another reference of Chueh et al.[18] for the surface reaction resistance yields very similar values, where the surface reaction resistance has been determined for patterned thin-film electrodes based on SDC ($Sm_{0.2}Ce_{0.8}O_{1.9-\delta}$). The surface reaction impedance for $p_{\mathrm{H_2}} = 0.13\,\mathrm{atm}$, $x_{\mathrm{H_2O}} = 0.0057\,\mathrm{atm}$ and a reaction site density of $A_R = 0.75$ was measured to be approximately $R_{\mathrm{SR,TF,pattern}} = 10\,\Omega\mathrm{cm}^2$.

Despite the uncertainties (operating conditions, different ceria compositions, thin-film v.s. porous material etc.) of these estimation, it can serve as reference to fit the right order of magnitude of the surface reaction resistance.

K Peak frequency of the gas diffusion impedance process

In Fig. 10 b) of the research article it is illustrated that the uncoupled gas diffusion impedance process with a peak frequency around 2 kHz is forced to the frequency range of the surface reaction resistance / chemical capacitance process below 1 Hz. In this section, experimental examples from literature illustrating this observation shall be discussed. Moreover, the order of magnitude of the frequency range for the uncoupled gas diffusion impedance process is confirmed by an analytical estimation.

Primdahl and Mogensen[19] performed EIS measurements on button cell configurations with pronounced gas diffusion effects. The EIS-spectra of the symmetric Ni/YSZ cell is shown in Fig. 3. In this configuration, the gas diffusion impedance process has a peak frequency around 25 Hz and is visible as a well distinguishable process, because the HOR-process is in the kHz-regime. This is an example for a gas diffusion impedance process considerably above 1 Hz.

The peak frequency of a gas diffusion impedance can be estimated by the following equation[19]:

$$f_0 = \frac{2.53 \cdot D_{\mathrm{eff}}}{2\pi {L_{\mathrm{Diff}}}^2} \tag{62}$$

where L_{Diff} is the diffusion length and D_{eff} the effective diffusion coefficient. This estimation provided reasonable agreement with measurements for the data of Primdahl and Mogensen[19]. In order to estimate the expected peak frequency for the uncoupled gas impedance process in Fig. 10 b) of the research article, we estimate an average diffusion coefficient for

the stagnant gas layer and the porous electrode:

$$D_{\text{eff}} = J_{\text{H}_2} \frac{L_{\text{Diff}}}{\Delta c_1} \tag{63}$$

where J_{H_2} is the hydrogen molar flux and Δc_1 is the total hydrogen concentration change over the diffusion length L_{Diff} from the simulation results. For the diffusion length L_{Diff} the sum of the stagnant gas layer and electrode thickness is used: $L_{\text{Diff}} = L_{\text{Stag}} + L$.

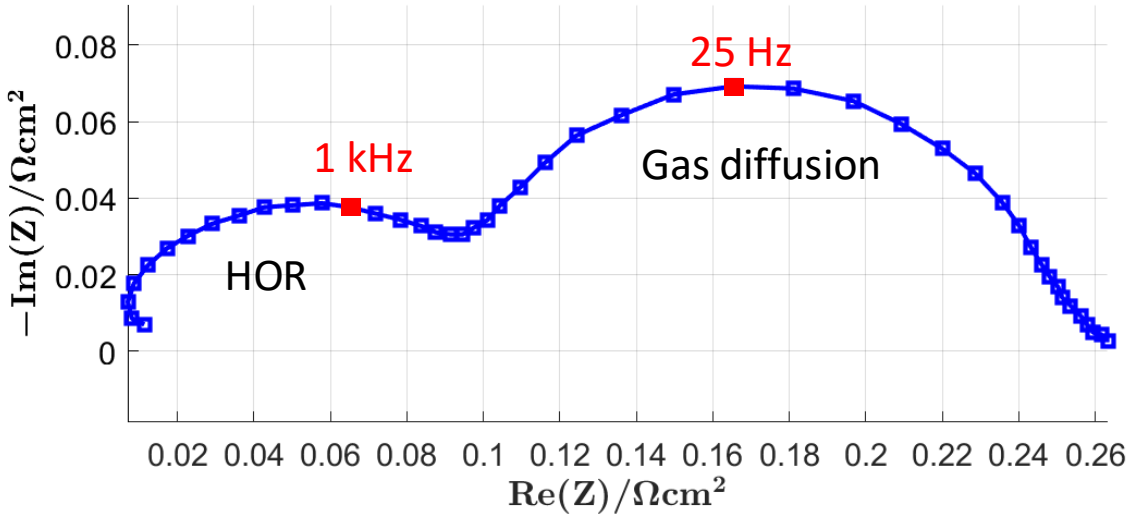

Fig. 3 Impedance spectra of a symmetric Ni/YSZ anode cell, manually extracted from Primdahl and Mogensen[19]. The spectra was measured in hydrogen with a water content of 3% at $T = 1'000°\text{C}$ at OCV. The arc with the peak frequency of 25 Hz was identified as a gas diffusion process and the arc around 1 kHz as a HOR-process.

With this procedure, the expected peak frequency of the uncoupled gas diffusion process is estimated to $f_0 = 451\,\text{Hz}$, which is in the same order of magnitude as the peak frequency $f_0 = 2'000\,\text{Hz}$ from the simulation. This crude estimation confirms that the uncoupled gas diffusion impedance process is far above the frequency range of the surface reaction resistance / chemical capacitance process below 1 Hz but is shifted to this frequency due to the coupling described in section 4.3 of the research article.

As an experimental example for the case of coupled processes for gas impedance and HOR, an EIS-spectra for a full cell with an Ni/CGO anode from Riegraf et al.[20] is shown in Fig. 4. The process with the peak frequency of about 0.2 Hz was identified as a mixed HOR and gas impedance process, as described in section 4.3 of the research article. The gas impedance in this setup with $4x4\text{cm}^2$ active area might be a combination of a gas conversion and a gas diffusion process. The gas conversion impedance process, which is neglected in the simulation model formulated for smaller button cells, might even have an intrinsic (uncoupled) peak frequency in the same range near $f_0 = 1\,\text{Hz}$. Gas conversion impedance processes in the frequency range of 1 Hz were e.g. reported by Primdahl and Mogensen[19,21]. However, as there is no gas process visible at higher frequencies, we conclude that the gas diffusion process and probably also the gas conversion process is forced to the frequency range of the surface reaction resistance / chemical capacitance process at about 0.2 Hz. Therewith, this example represents a experimental realization of the coupling of these processes discussed in section 4.3 of the research article.

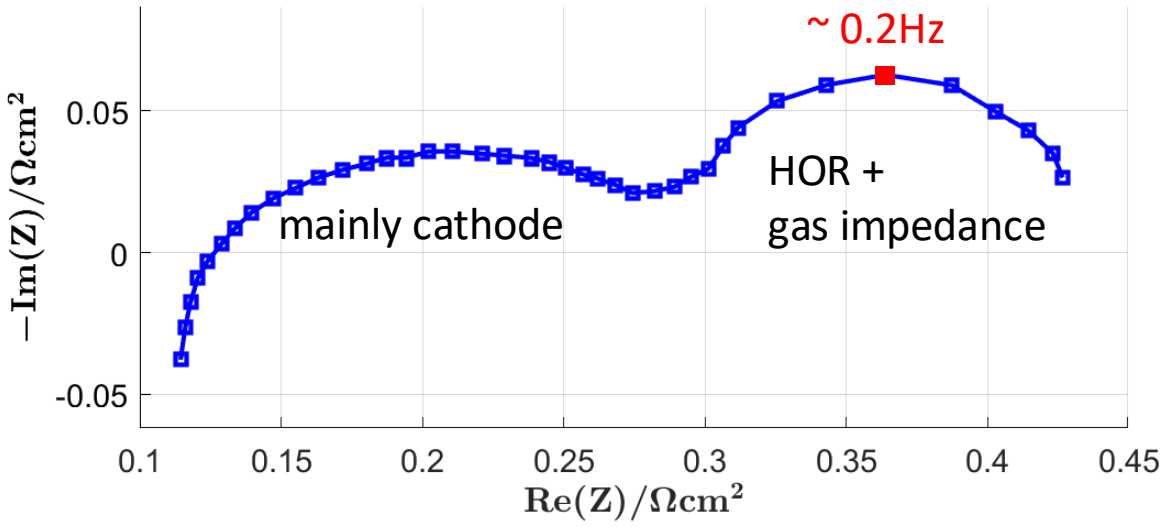

Fig. 4 EIS spectra of a $4x4\mathrm{cm}^2$ full cell with Ni/CGO anode, manually extracted from Riegraf et al.[20]. The spectra was measured in hydrogen with a water content of 9% at $T = 850°\mathrm{C}$ at OCV. The process with the peak frequency of $0.2\,\mathrm{Hz}$ was identified as a mixed HOR and gas impedance process.

Notes and references

1 T. Nakamura, K. Yashiro, A. Kaimai, T. Otake, K. Sato, T. Kawada and J. Mizusaki, *Journal of The Electrochemical Society*, 2008, **155**, B1244–B1250.

2 M. Linder, T. Hocker, R. Denzler, A. Mai and B. Iwanschitz, Fuel Cells, 2011, pp. 573–580.

3 R. Krishna and J. A. Wesselingh, *Chemical Engineering Science*, 1997, **52**, 861–911.

4 A. Bertei and C. Nicolella, *Journal of Power Sources*, 2015, **279**, 133–137.

5 M. Kishimoto, M. Lomberg, E. Ruiz-Trejo and N. P. Brandon, *Electrochimica Acta*, 2016, **190**, 178–185.

6 S. Liu, W. Kong and Z. Lin, *Journal of Power Sources*, 2009, **194**, 854–863.

7 R. Suwanwarangkul, E. Croiset, M. W. Fowler, P. L. Douglas, E. Entchev and M. A. Douglas, *Journal of Power Sources*, 2003, **122**, 9–18.

8 R. Suwanwarangkul, E. Croiset, E. Entchev, S. Charojrochkul, M. D. Pritzker, M. W. Fowler, P. L. Douglas, S. Chewathanakup and H. Mahaudom, *Journal of Power Sources*, 2006, **161**, 308–322.

9 B. Todd and J. B. Young, *Journal of Power Sources*, 2002, **110**, 186–200.

10 E. N. Fuller, P. D. Schettler and J. C. Giddings, *Industrial and Engineering Chemistry*, 1966, **58**, 18–27.

11 J. Becker, C. Wieser, S. Fell and K. Steiner, *International Journal of Heat and Mass Transfer*, 2011, **54**, 1360–1368.

12 GeoDict, *Math2Market GmbH*, 2019, `www.geodict.com`.

13 X. Lu, B. Tjaden, A. Bertei, T. Li, K. Li, D. Brett and P. Shearing, *Journal of the Electrochemical Society*, 2017, **164**, F188–F195.

14 B. C. Steele, *Solid State Ionics*, 2000, **129**, 95–110.

15 I. Yasuda and M. Hishinuma, Ionic and Mixed Conducting Ceramics, International Symposium, 3, Meeting of the Electrochemical Society, 192, Electrochemical Society Proceedings Volume, 1998, pp. 178–187.

16 S. Wang, T. Kobayashi, M. Dokiya and T. Hashimoto, *ECS Proceedings*, 2000, **99**, 193 – 200.

17 M. Gerstl, A. Hutterer, J. Fleig, M. Bram and A. K. Opitz, *Solid State Ionics*, 2016, **298**, 1–8.

18 W. C. Chueh, Y. Hao, W. Jung and S. M. Haile, *Nature Materials*, 2012, **11**, 155–161.

19 S. Primdahl, *Journal of The Electrochemical Society*, 1999, **146**, 2827.

20 M. Riegraf, V. Yurkiv, R. Costa, G. Schiller and K. A. Friedrich, *ChemSusChem*, 2017, **10**, 587–599.

21 M. Primdahl, S; Mogensen, *Journal of The Electrochemical Society*, 1998, **145**, 2431.